# Long-Range Ordering of Block Copolymer Cylinders Driven by Combining Thermal Annealing and Substrate Functionalization

**Ming-Shiuan She,[†] Ting-Ya Lo,[†] and Rong-Ming Ho[†,‡,*]**

[†]Department of Chemical Engineering, National Tsing Hua University, Hsinchu 30013, Taiwan, Republic of China, and [‡]Frontier Research Center on Fundamental and Applied Sciences of Matters, National Tsing Hua University, Hsinchu, 30013, Taiwan, Republic of China

**ABSTRACT** This work presents a new method for forming well-defined nanostructured thin films from self-assembled polystyrene-*block*-poly(L-lactide) (PS-PLLA) on Si wafers with a functionalized $SiO_2$ surface. Large, well-ordered, perpendicular PLLA cylinders in PS-PLLA thin films can be formed using the functionalized substrate. In contrast to random copolymers, a neutral substrate for the PS and PLLA blocks is formed by functionalizing a substrate with hydroxyl-terminated PS (PS-OH) followed by hydroxyl-terminated PLLA (PLLA-OH). The heterogeneous grafting of PS-OH and PLLA-OH can be substantially alleviated using this two-step functionalization. Accordingly, the surface properties can be fine-tuned by controlling the ratio of grafted PS-OH to PLLA-OH to control the orientation of the PLLA cylinders on the functionalized $SiO_2$. Nevertheless, the orientation that is driven by the neutral substrate is surprisingly limited in that the effective length of orienting cylinders is less than twice the interdomain spacing. Thermal annealing at high temperature can yield a neutral air surface, rendering perpendicular PLLA cylinders that stand sub-micrometers from the air surface. Consequently, the neutral substrate can be used to enable truly film-spanning perpendicular cylinders in films to be fabricated using the high-temperature thermal treatment. In addition, the perpendicular cylinders can be laterally ordered by further increasing the annealing temperature. The ability to create these film-spanning perpendicular cylinders in films with a well-ordered texture and sub-micrometer thickness opens up possible applications in nanotechnology.

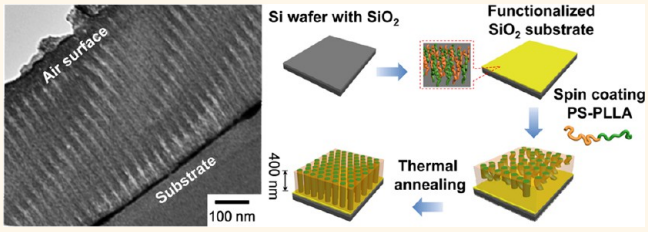


**KEYWORDS:** mixed homopolymer brushes · thin films · degradable block copolymers · orientation

In recent decades, block copolymers (BCPs) have been extensively investigated because of their ability to self-assemble into various ordered nanostructures, such as spheres, cylinders, gyroids, and lamellae. The self-assembly results from incompatibility of their constituent blocks.[1,2] Well-defined nanostructured phases can be tailored by the molecular engineering of synthetic BCPs, with promising features for nanotechnological applications. For such nanostructured materials to prove useful in applications, thin-film samples with oriented periodic arrays over large areas must be formed. Different approaches for controlling the orientation of phase-separated microdomains have been developed. They include solvent evaporation,[3−6] solvent annealing,[7−9] the application of shear fields,[10−16] the application of electric fields,[17−19] the use of temperature gradients,[20,21] epitaxial crystallization,[22−24] chemical patterning of the surface,[25−31] and graphoepitaxy.[32−43] The use of chemically neutral surfaces has been one of the most commonly used approaches.[44−53] For two-component systems (denoted A and B) at interfaces, the interfacial energy difference may be defined as $\Delta\gamma = \gamma_A - \gamma_B$. When $\gamma_A = \gamma_B$, the interactions between the polymers and the surface are balanced and the surface is neutral.[49,54] The interactions between a chemically neutral surface and each block of a given copolymer can be balanced to form oriented microdomains of self-assembled BCPs.

A variety of methods have been demonstrated to provide neutral surfaces such that well-oriented BCP microdomains can be formed in thin films.[44−48] The most common approach for establishing chemical neutrality is to treat the substrate with a

* Address correspondence to rmho@mx.nthu.edu.tw.

Received for review August 25, 2012 and accepted February 25, 2013.

**Published online February 25, 2013**
10.1021/nn305725q

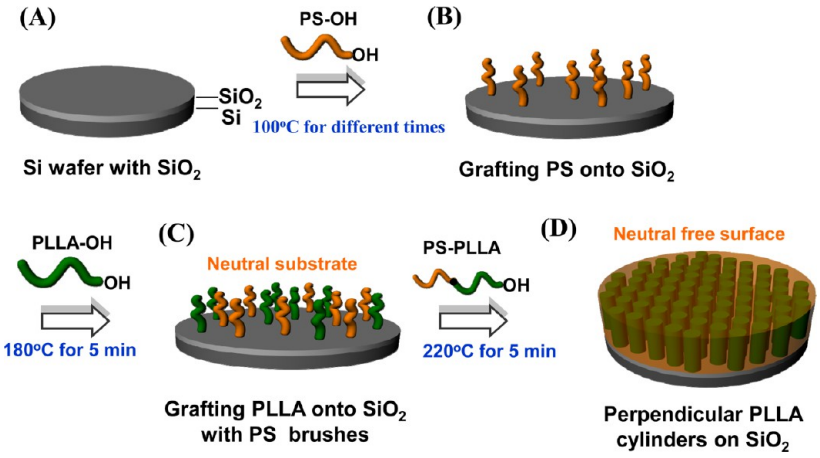


**Figure 1. Schematic illustration of the preparation of neutral substrate and the formation of neutral free surface for the fabrication of well-oriented perpendicular cylindrical nanostructures from self-assembled PS-PLLA. (A) Si wafer with $SiO_2$; (B) functionalized $SiO_2$ by using PS-OH through thermal annealing; (C) functionalized $SiO_2$ with both PS-OH and PLLA-OH brushes through thermal annealing; (D) perpendicular PLLA cylinders on functionalized $SiO_2$ surface with PS-OH and PLLA-OH brushes (neutral substrate for PS-PLLA).**

random copolymer brush layer that contains the same monomer units as the block copolymer.[49−53] However, the synthesis of such random copolymers may not be easy or even impossible for some monomer pairs. Recently, Nealey *et al.* demonstrated a method for preparing neutral brush layers by using a ternary blend that consists of two low-molecular-weight homopolymers and a corresponding low-molecular-weight block copolymer to replace synthesized random copolymers for the formation of neutral substrates.[53] Furthermore, Russell *et al.* investigated the use of BCP brushes, rather than random copolymer brushes, to control the orientation of BCP microdomains in thin films.[55]

This study aims to develop a new method that uses homopolymers with hydroxyl groups at the ends of the chains to functionalize a $SiO_2$ surface to form well-defined nanostructured thin films of polystyrene-*block*-poly(L-lactide) (PS-PLLA) with PLLA cylinders on a Si wafer with a $SiO_2$ surface. As illustrated in Figure 1, the formation of functionalized substrate (the neutral substrate for the PS and PLLA blocks) can be achieved by two-step functionalization. Homogeneously functionalized $SiO_2$ can be obtained using PS-OH through thermal annealing at 100 °C, followed by functionalization using PLLA-OH through thermal annealing at 180 °C. As a result, the surface properties can be fine-tuned by controlling the the ratio of grafted PS-OH to PLLA-OH using this new method. Unlike direct functionalization using a mixture of PS-OH and PLLA-OH, which would cause the problem of phase separation during the annealing process due to the incompatibility between the PS and the PLLA so as to result in heterogeneous grafting, the two-step method that is developed herein provides homogeneous and uniform grafting. The formation of a neutral substrate without the need for random copolymer synthesis is a simple means of forming nanostructured thin films from self-assembled block copolymers. Nevertheless, the effective thickness of the region of orientation that is induced by the neutral substrate is limited. Thermal annealing at high temperature can yield a neutral air surface, rendering perpendicular PLLA cylinders that stand far from the air surface. Combining thermal annealing at high temperature to form a neutral air surface with the use of the neutral substrate can form perpendicular PLLA cylinders with sub-micrometer thickness throughout the films.

Note that Nealey *et al.* demonstrated the feasibility to achieve similar results but using a random copolymer approach for the induced orientation of a non-crystallizable polystyrene-*block*-poly(methyl methacrylate) (PS-PMMA) BCP thin film.[47] By contrast, we demonstrate a new approach to control the orientation of cylindrical microdomains, in particular for semicrystalline block copolymers, and to achieve film-spanning cylinders with sub-micrometer thickness. It is also noted that, to facilitate the orientation of the PLLA cylinders in the PS-PLLA thin film, it is necessary to give the microphase-separated cylinders some orientation on the surface layer after spin-coating as the initial stage for the following ordering process. According to our previous work using solvent evaporation for the induction of oriented cylinders,[56,57] perpendicular racemic poly(D,L-lactide) (PLA) cylinders in polystyrene-*b*-poly(D,L-lactide) (PS-PLA) thin film cannot be easily formed by spin-coating because of the low segregation strength of the PS-PLA as compared to PS-PLLA.[58] As a result, we speculate that similar behavior and results will not be easily achieved by using PS-PLA as material. For semicrystalline BCPs such as PS-PLLA, this is indeed the first time to achieve the film-spanning cylinders with sub-micrometer thickness. Note that the crystallization of semicrystalline block copolymers would interrupt the orientation of the BCP nanostructured

phase, in particular driven by casting. Avoiding the crystallization effect is extremely critical to the microphase separation of self-assembled BCPs. That is the reason we used thermal annealing at high temperature to achieve the induced orientation without the perturbation of the crystallization event. Furthermore, the hexagonally packed cylinders can be laterally ordered by high-temperature thermal annealing. This work demonstrates a general and efficient means of producing large-scale, well-oriented nanoarrays in the form of thin films by using degradable block copolymers, which may be useful in functional block copolymer systems.

## RESULTS AND DISCUSSION

**Formation of Oriented PLLA Cylinders in PS-PLLA *via* Solvent Evaporation.** As reported in our previous studies, perpendicular PLLA cylinders in the PS-PLLA (its chemical structure is shown in Figure 2) thin film can be formed by selecting a solvent with the proper evaporation rate and high selectivity with constituted blocks of PS-PLLA.[56,57] To examine the limitation of the thickness of the region of oriented perpendicular PLLA cylinders in this approach, PS-PLLA thin films with thicknesses of 50 to 200 nm were prepared on a Si wafer with a $SiO_2$ surface by spin-coating at 50 °C using PS-PLLA solutions with different concentrations. In Figure 3, the top-view scanning probe microscope (SPM) phase image (Figure 3(a-top)) and bottom-view SPM phase image (Figure 3(a-bottom)) enable the cross-section of the cylindrical nanostructures to be clearly determined. These results suggest that vertically oriented cylindrical PLLA micordomains can be formed, spanning a thickness to a depth of 50 nm in the thin film. The top-view SPM phase images in Figure 3(b-top) and (c-top) for thin films with thicknesses of 100 and 150 nm, respectively, show similar results, but in the bottom-view SPM phase images (Figure 3(b-bottom) and (c-bottom)), the regions of disordered morphology gradually become larger. Further increasing the thickness of the thin film to 200 nm produces no significant microphase-separated morphology that can be observed in the bottom-view SPM phase image (Figure 3(d-bottom)), although the top-view SPM phase images continue to show the cross-section of the cylindrical nanostructures (Figure 3(d-top)). As a result, the perpendicular orientation of PLLA cylinders can be induced only by spin-coating in films of limited thickness. To fabricate thick PS-PLLA films with perpendicular PLLA cylindrical microdomains, a Si wafer with a $SiO_2$ surface was functionalized with PS and PLLA brushes to eliminate the limitation on the thickness in which the orientation can be induced. To facilitate the orientation of the PLLA cylinders in the PS-PLLA thin film, the microphase separation of PS-PLLA was first induced by spin-coating to provide the initial stage of ordering of the nanostructures in which perpendicular PLLA cylinders are present in the PS-PLLA thin films on the surface layer. Notably, a neutral substrate must be used to avoid preferential interaction of one block with the substrate, which would produce microdomains that are orientated parallel to the surface of the film. Therefore, the neutral substrate was created herein by functionalizing the substrate with hydroxyl-terminated PS (PS-OH) and hydroxyl-terminated PLLA (PLLA-OH) brushes.

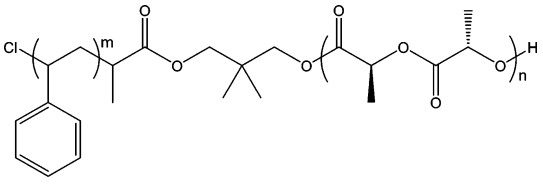


Figure 2. Chemical structure of PS-PLLA.

**Functionalization of $SiO_2$.** To reduce the heterogeneous grafting of PS-OH and PLLA-OH by direct functionalization

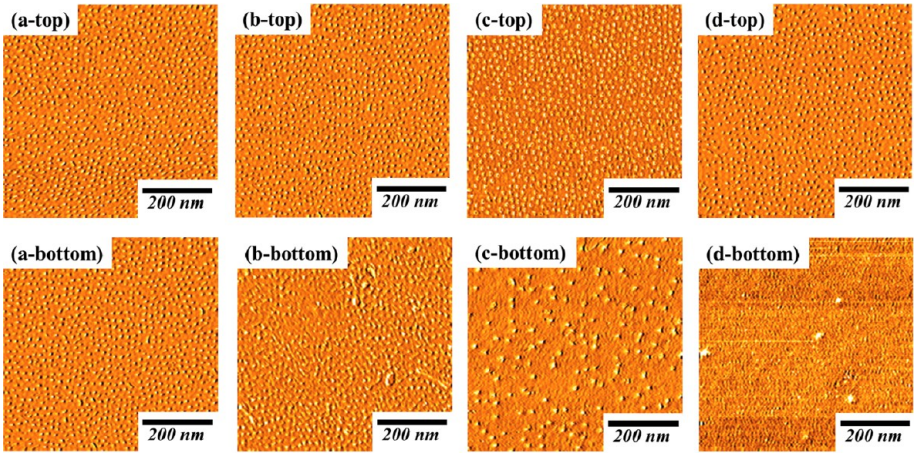


Figure 3. Tapping-mode (a-top–d-top) top-view and (a-bottom–d-bottom) bottom-view SPM phase images of PS-PLLA thin films with a thickness of 50 nm (a-top, a-bottom), 100 nm (b-top, b-bottom), 150 nm (c-top, c-bottom), and 200 nm (d-top, d-bottom) after spin-coating at 50 °C.

**TABLE 1. Characterization of $SiO_2$ Surface Functionalized with PS-OH and PLLA-OH**

| substrate | time (min)[a] | $\theta_{w\ PS}$ (deg)[b] | $\theta_{e\ PS}$ (deg)[c] | $\theta_{w\ PSandPLLA}$ (deg)[b] | $\theta_{e\ PSandPLLA}$ (deg)[c] | $C_{1s}$ | $O_{1s}$ | $Si_{2p}$ | $O_{1S}$ (PLLA)[d] | $O_{1S}$ (PLLA) %[e] | PLLA%[f] |
|---|---|---|---|---|---|---|---|---|---|---|---|
| SUB-1 | 30 | 62.3 | 47.2 | 71.4 | 51.1 | 38.41 | 44.91 | 16.67 | 11.57 | 23.1 | 35.5 |
| SUB-2 | 60 | 65.2 | 50.1 | 73.2 | 52.5 | 19.03 | 55.87 | 25.1 | 5.67 | 22.9 | 35.0 |
| SUB-3 | 90 | 70.5 | 55.2 | 74.5 | 53.2 | 19.75 | 55.2 | 25.05 | 5.1 | 20.5 | 29.7 |
| SUB-4 | 120 | 79.1 | 56.1 | 81.2 | 56.3 | 47.4 | 38.56 | 14.04 | 10.48 | 18.1 | 24.9 |
| SUB-5 | 150 | 83.8 | 58.3 | 83.4 | 58.3 | 43.94 | 39.72 | 16.34 | 7.04 | 13.8 | 17.4 |
| SUB-6 | 180 | 84.4 | 58.7 | 84.6 | 59.3 | 46.38 | 36.45 | 17.17 | 2.11 | 4.3 | 4.7 |

[a] The $SiO_2$ surface was functionalized with PS-OH brushes by thermal annealing. [b] Water contact angle measurements were carried out on the $SiO_2$ surface functionalized with PS-OH or mixed PS-OH and PLLA-OH brushes. [c] Ethylene glycol contact angle measurements were carried out on the $SiO_2$ surface functionalized with PS-OH or mixed PS-OH and PLLA-OH brushes. [d] $O_{1S}(PLLA) = O_{1s} - O_{1s}(SiO_2) = O_{1s} - 2Si_{2p}$. [e] Oxygen atomic compositions were calculated from XPS measurements for functionalized $SiO_2$ surface with PS-OH and PLLA-OH brushes. C % + O % = 100%. [f] PS−OH% + PLLA% = 100%.

that is caused by the incompatibility of PS-OH with PLLA-OH, a two-step grafting procedure was used. The process begins with the grafting of PS-OH onto the surface of $SiO_2$ by thermal annealing. The temperature for grafting PS-OH was 140 °C, and the grafting was conducted in a vacuum. This temperature was well above the glass transition temperature ($T_g$) of PS to enable the hydroxyl-terminated PS to diffuse to and react with the $SiO_2$ on top of the Si wafer. Also, the grafting density of the PS-OH on the $SiO_2$ surface was controlled by varying the thermal annealing time. To determine the variation in the surface tension of the functionalized $SiO_2$ surfaces with annealing time, contact angle measurements were made using water as a testing material. The dependence of the contact angle on annealing time at 140 °C reveals a rapid increase in the first stage of annealing to a plateau of less than 5 min (not shown here), suggesting that the hydroxyl groups on the $SiO_2$ surface reacted with the end-hydroxyl group of PS, and this reaction was complete in 5 min. To slow the reaction to gain more control of the grafting rate, the substrates with the thin layer of PS-OH homopolymer were then treated at 100 °C, which is slightly above the $T_g$ of PS, in thermal annealing for 30, 60, 90, 120, 150, and 180 min. The substrates thus obtained are labeled SUB-1, SUB-2, SUB-3, SUB-4, SUB-5. and SUB-6, respectively. As shown in Table 1, the water contact angle for functionalized $SiO_2$ following annealing at a temperature of 100 °C gradually increases with annealing time, suggesting that the surface energy of the $SiO_2$ surface that is functionalized with PS-OH brushes can be reasonably controlled by thermal annealing at 180 °C. Following the functionalization of $SiO_2$ with PS-OH, PLLA-OH was covalently grafted on the functionalized $SiO_2$ by thermal annealing. The hydroxyl-terminated PLLA reacted with the residual hydroxyl group of the functionalized $SiO_2$, forming mixed homopolymer brushes. Notably, PLLA-OH is a crystalline polymer and may be crystallized by thermal annealing in the temperature range from 60 °C to approximately 180 °C. Accordingly, the thermal treatment had to be conducted above the melting temperature of PLLA to avoid crystallization. As a result, the reaction temperature for grafting PLLA-OH on the functionalized $SiO_2$ with PS-OH was 180 °C.

**Surface Analysis of Functionalized $SiO_2$.** To examine the surface compositions of mixed homopolymer brushes on the $SiO_2$ surfaces, X-ray photoelectron spectroscopy (XPS) measurements were made. Figure 4 shows a survey scan and the $C_{1S}$ spectrum of the $SiO_2$ surfaces with mixed homopolymer brushes. As shown in Figure 4A, in addition to the oxygen (533 eV) and carbon (285 eV) signals, a $Si_{2p}$ peak is found at 103.4 eV and is attributed to $SiO_2$, suggesting that the oxygen signal is attributed to the formation of PLLA and the $SiO_2$ layer. Figure 4B shows the $C_{1s}$ spectra of $SiO_2$ that was functionalized with PS-OH, PLLA-OH, and mixed PS-OH and PLLA-OH brushes (as obtained using the SUB-1 sample).

The spectra include the $C_{1s}$ peak at 285.0 eV that corresponds to the carbon atoms in saturated hydrocarbons (−C−H−) of PS-OH and PLLA-OH. Also, the $C_{1s}$ shakeup peak (peak d), corresponding to the $\pi-\pi^*$ transition of the PS-OH benzene ring, was observed at approximately 291.5−292.0 eV.[59] Peaks b and c, observed at 286.5 and 289 eV, were assigned to the carbon atoms with a single bond to oxygen (−O−C−) and carbonyl groups (−C═O−) of PLLA-OH, respectively.[60] Those characteristic peaks can also be found in the $C_{1s}$ spectra of SUB-2, SUB-3, SUB-4, SUB-5, and SUB-6 (not shown here). As a result, the XPS results demonstrate that the PS-OH and PLLA-OH brushes were successfully grafted onto the surface of $SiO_2$ (Figure 4B). To characterize the variation of the proportion of PLLA-OH on the $SiO_2$ surface by thermal annealing for different annealing times, the atomic composition ratio was calculated from the XPS results. As mentioned above, the oxygen signal is attributed to the PLLA homopolymers and $SiO_2$. To calculate precisely the proportion of PLLA, the signal of the oxygen atoms that correspond to the $SiO_2$ was subtracted from the oxygen signal in the XPS spectra. Table 1 summarizes the results. The calculated proportion of PLLA decreased from 35.5% to 4.7% as the thermal annealing time increased from 30 to 180 min in the process of grafting the PS-OH brushes. The results indicate that

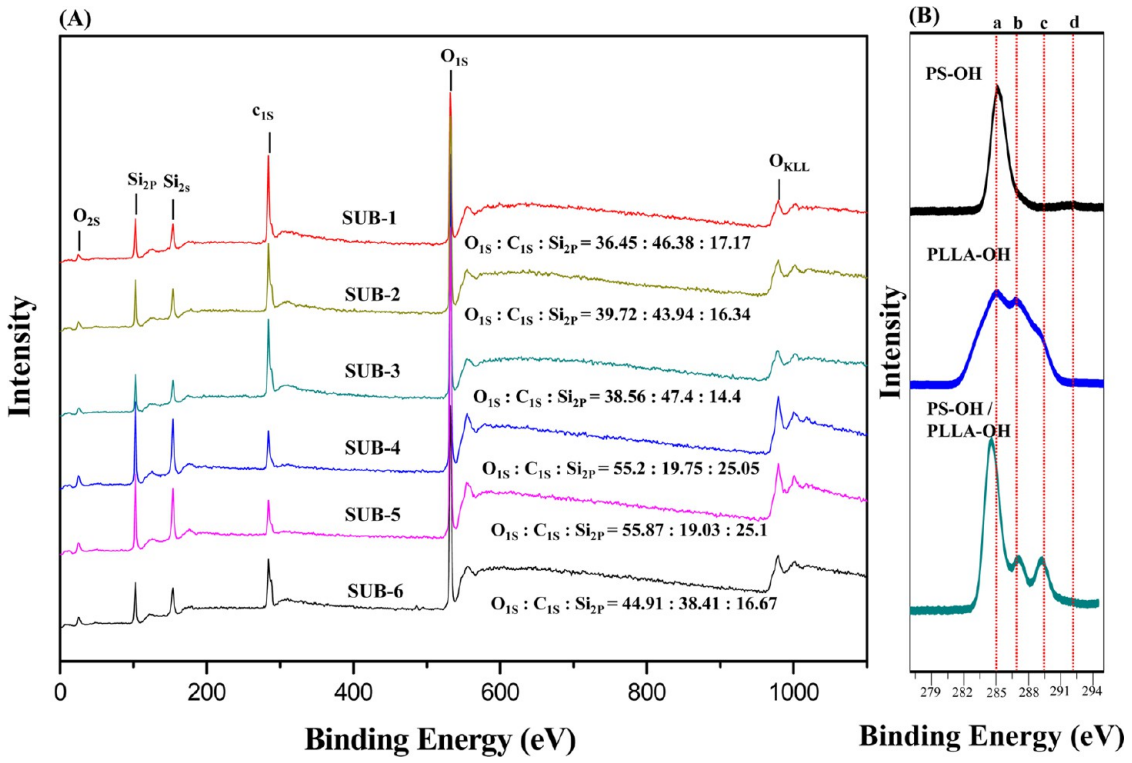


**Figure 4. (A) XPS survey spectra of functionalized $SiO_2$ by using PS-OH brushes through thermal annealing at 30 (SUB-1), 60 (SUB-2), 90 (SUB-3), 120 (SUB-4), 150 (SUB-5), and 180 (SUB-6) min followed by grafting PLLA-OH brushes. (B) $C_{1s}$ XPS spectra of PS-OH, PLLA-OH, and mixed PS-OH and PLLA-OH brushes on a $SiO_2$ surface.**

the composition ratio of PS-OH to PLLA-OH on the $SiO_2$ surface can be effectively controlled by this two-step annealing process.

As demonstrated above, functionalized $SiO_2$ surfaces with different composition ratios of PS to PLLA brushes can be prepared by controlling the two-step grafting procedure by varying the thermal annealing conditions. To investigate the variation of the surface tension of the functionalized $SiO_2$ surface and also the affinity of the surface for PS and PLLA components, the adhesion of functionalized $SiO_2$ to PS ($W_{PS\text{-}Sub}$) and PLLA ($W_{PLLA\text{-}Sub}$) was calculated. Figure 5 plots $W_{PS\text{-}Sub}$ and $W_{PLLA\text{-}Sub}$ as functions of functionalized $SiO_2$ with PS fraction ($f_{PS}$). As $f_{PS}$ increases, $W_{PS\text{-}Sub}$ increases rapidly to 49 mJ $m^{-2}$ at $f_{PS} = 0.65$; thereafter, it further increases to a plateau of 55 mJ $m^{-2}$ at $f_{PS} > 0.7$. In contrast, $W_{PLLA\text{-}Sub}$ falls slightly as $f_{PS}$ increases. $W_{PS\text{-}Sub}$ will be approximately equal to $W_{PLLA\text{-}Sub}$ at $f_{PS} = 0.75$. We speculate that the interactions between the polymers and the functionalized $SiO_2$ can be balanced once the $f_{PS}$ reaches 0.75 because of the formation of a neutral substrate.

**Orientation Induced by Functionalized Surface.** To examine the feasibility of the two-step grafting approach for forming a neutral substrate, a PS-PLLA thin film with a thickness of 50 nm was spin-coated onto the functionalized $SiO_2$ surface. Notably, the effect of the substrate on the forming morphology from the self-assembly of BCPs is thermodynamically driven.

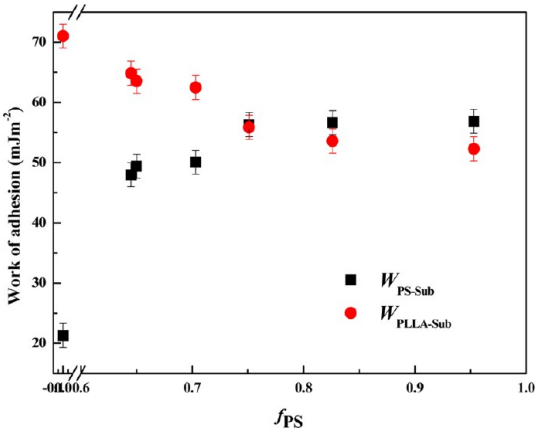


**Figure 5. Work of adhesion for $W_{PS\text{-}Sub}$ (squares) and $W_{PLLA\text{-}Sub}$ (circles) on the functionalized $SiO_2$ surface with PS-OH and PLLA-OH brushes.**

To achieve a stable equilibrium state, the morphology of the as-cast BCP thin film with disordered nanostructure requires longer annealing time than that with a well-developed cylindrical nanostructure. Consequently, as mentioned above, the sample that was solution-cast using a selective solvent was used to create an initially ordered morphology to expedite the process in which the stable morphology is reached. Also, the thin-film sample was annealed at 140 °C above $T_g$ of PS to initiate the morphological evolution. As shown in Figure 6, the bottom-view images of both

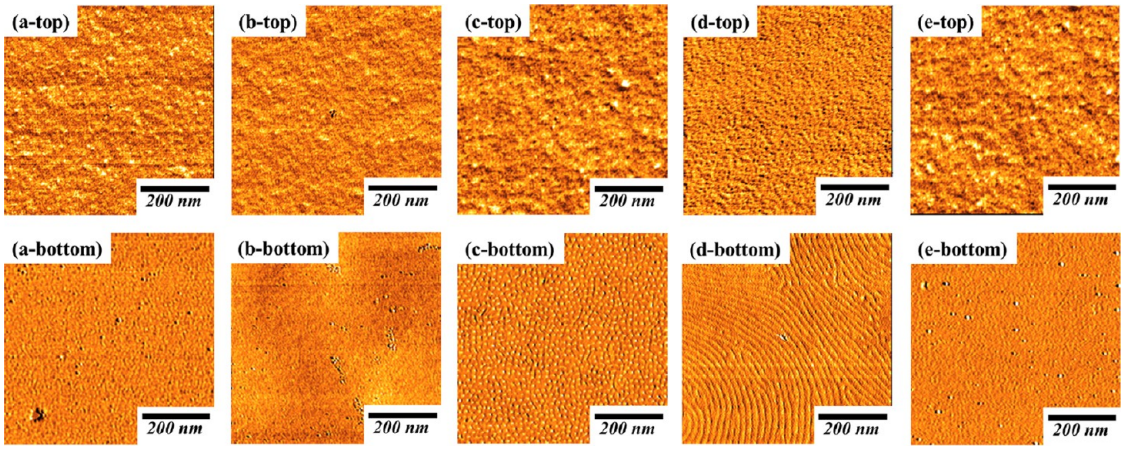


**Figure 6. Tapping-mode (a-top−e-top) top-view and (a-bottom−e-bottom) bottom-view SPM phase images of PS-PLLA thin films with a thickness of 50 nm on functionalized $SiO_2$ of SUB-1 (a-top, a-bottom), SUB-2 (b-top, b-bottom), SUB-3 (c-top, c-bottom), SUB-4 (d-top, d-bottom), and SUB-5 (e-top, e-bottom) with thermal annealing at 140 °C for 5 min.**

SUB-1 and SUB-2 show no significant microphase-separated morphology in PS-PLLA thin films following thermal annealing at 140 °C. Furthermore, the morphology at the bottom of SUB-1 appears to be that of a well-defined nanostructure only when the film was treated by hydrolysis (degradation of PLLA) (Figure S1), suggesting that a thin layer of PLLA is formed on the substrate. Similar results (not shown) are found for thin films on functionalized $SiO_2$ of SUB-2. We thus speculate that the preferential wetting of PLLA on SUB-1 and SUB-2 is mainly attributed to the affinity effect by which both SUB-1 and SUB-2 exhibit preferential selectivity toward the PLLA microdomain. In contrast, the formation of perpendicular cylinders is identified in SUB-3 from the SPM bottom-view image (Figure 6(c-bottom)), suggesting the effect of a neutral substrate (as expected based on the calculated results concerning the work of adhesion) on the formed morphology. Nevertheless, no clear microphase-separated texture is found in the SPM top-view image (Figure 6(c-top)). This morphological observation surprisingly indicates that the effective length of induced cylinder orientation by the neutral substrate is extremely limited because the thickness of the thin film is only 50 nm, approximately twice the interdomain spacing. In the thin film that was cast onto the substrate that was slightly selective toward the PS microdomain (SUB-4), parallel cylinders (Figure 6(d-bottom)) are observed. The formed morphology is very sensitive to the selectivity of the used substrate, so the thin layer of PS (Figure 6(e-bottom)) will be formed on the substrate with preferential selectivity to the PS domain (SUB-5), and the microphase-separated morphology in PS-PLLA thin films cannot be seen even with hydrolytic treatment. The results obtained from the SPM top-view images of Figure 6 are consistent with the behavior as described above and the fact that the effect of the substrate on the formation of the microphase-separated morphology from the air surface is insignificant. As the thickness of the thin film increases above 50 nm (to, for example, 100 and 200 nm), similar results (not shown) with respect to the effect of the substrate can be found. Consequently, the orientation of the cylindrical domain can be effectively controlled on the functionalized $SiO_2$ surfaces, but the effective thickness is very limited.

**Orientation Induced by Thermal Annealing.** Notably, the orientation of the cylindrical domain in the BCP thin film and the corresponding lateral order can be tuned by controlling the annealing temperature to achieve the most stable morphologies.[47,54] To examine the effect of annealing on the formation of BCP nanostructures by spin-coating, PS-PLLA thin films were thermally annealed over the $T_g$ of the PS in this study. When the annealing temperature is lower than 140 °C, the observed morphology does not change significantly. As the annealing temperature increases from 140 to 160 °C (Figure 7), the bottom-view images are consistent with the phenomenon, as described above, by which the cylindrical domain is oriented by the functionalized $SiO_2$ surface (Figure 7(c-bottom)). In contrast, the microphase-separated morphology in the top-view images is slightly changed, indicating that thermal annealing is beginning to have an effect. As the annealing temperature approaches 180 °C, the morphology of the BCP thin film varies significantly. The formation of perpendicular cylinders driven by thermal annealing, resulting from the formation of a neutral air surface, is clearly identified in the top-view images in Figure 8. Similar bottom-view images in Figures 7 and 8 reveal the effect of the substrate. They indicate that orientation of the cylindrical domain controlled by thermal annealing has no impact on the effect of the substrate on the thin-film morphology between the BCP and the functionalized substrate. The induced orientation from the air surface is attributed to the effect of temperature on the surface tensions of PS ($\gamma_{PS}$) and PLLA ($\gamma_{PLLA}$). In the PS-PLLA system, PLLA has

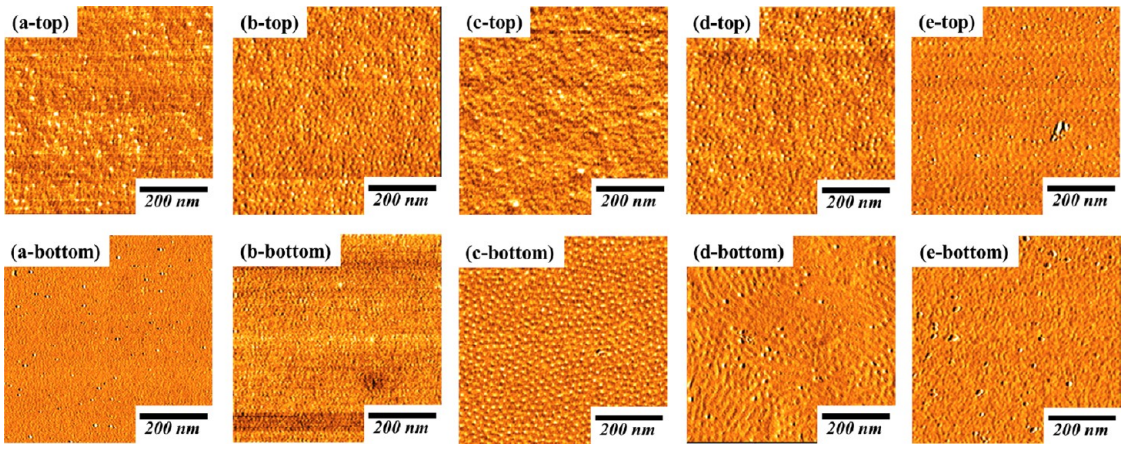


**Figure 7. Tapping-mode (a-top−e-top) top-view and (a-bottom−e-bottom) bottom-view SPM phase images of PS-PLLA thin films with a thickness of 50 nm on functionalized $SiO_2$ of SUB-1 (a-top, a-bottom), SUB-2 (b-top, b-bottom), SUB-3 (c-top, c-bottom), SUB-4 (d-top, d-bottom), and SUB-5 (e-top, e-bottom) with thermal annealing at 160 °C for 5 min.**

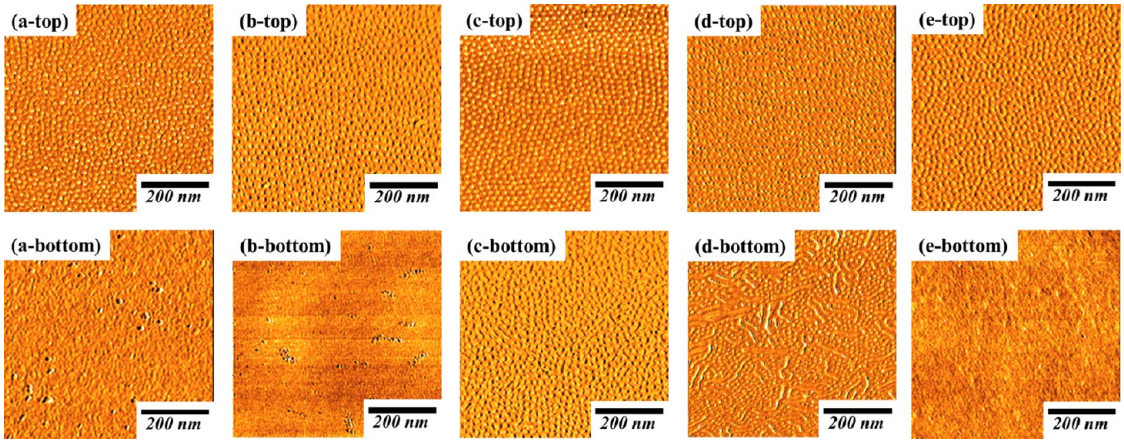


**Figure 8. Tapping-mode (a-top−e-top) top-view and (a-bottom−e-bottom) bottom-view SPM phase images of PS-PLLA thin films with a thickness of 50 nm on functionalized $SiO_2$ of SUB-1 (a-top, a-bottom), SUB-2 (b-top, b-bottom), SUB-3 (c-top, c-bottom), SUB-4 (d-top, d-bottom), and SUB-5 (e-top, e-bottom) with thermal annealing for 5 min at 180 °C.**

a lower surface tension (38.3 mN/m) than PS (40.7 mN/m) at room temperature.[61] Also, $\gamma_{PS}$ and $\gamma_{PLLA}$ decrease as the temperature increases. We speculate that the rate of decrease of $\gamma_{PS}$ with increasing temperature is higher than that of $\gamma_{PLLA}$, yielding equal values of $\gamma_{PS}$ and $\gamma_{PLLA}$ at high annealing temperature. Surface energies of the two constituent blocks of a diblock copolymer reportedly lead to the formation of perpendicular cylinders in BCP thin films.[47,61,62] Consequently, perpendicular PLLA cylinders in PS-PLLA thin film can be formed by thermal annealing at 180 °C.

**Induced Long-Range Perpendicular Orientation.** Based on the findings above, an attempt is made to generate perpendicular PLLA cylinders in thicker films (thickness >100 nm). Figure 9(a-top) and (a-bottom) show the SPM top-view phase and bottom-view phase of a PS-PLLA thin film with a thickness of 100 nm on SUB-3 substrate following thermal annealing. Similar results can be found for thin films with a thickness of 200 nm, as shown in Figure 9(b-top) and (b-bottom). As a result, perpendicular cylinders throughout the 100 and 200 nm thickness of the BCP film on the neutral substrate can be formed by thermal annealing. To examine the limitation of the induced perpendicular orientation, thicker thin-film samples were thermally annealed at 180 °C. Similar SPM results were obtained for the sample with a thickness of 400 nm (Figure 9(c-top) and (c-bottom)). To examine further the suggested perpendicular cylinders that span the entire thickness of the film, the orientation of the microdomain in the film on the functionalized $SiO_2$ surface was determined from SPM top-view and bottom-view images of the films following progressive oxygen plasma etching steps from the top and from the bottom of the films. Figure S2 shows the SPM results following oxygen plasma etching for different etching times. The top-view phase images following oxygen plasma etching from the top downward for 60 s in Figure S2(a) reveal well-ordered perpendicular cylindrical domains on the surface of the thin film with a thickness of 300 nm. Further increasing the etching time to 90 s yields a thin-film sample with a thickness of

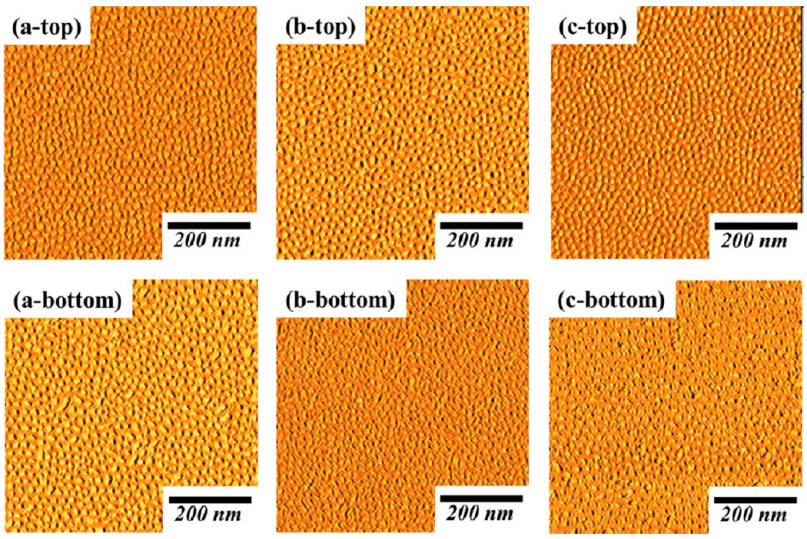


**Figure 9. Tapping-mode (a-top, b-top, c-top) top-view and (a-bottom, b-bottom, c-bottom) bottom-view SPM phase images of PS-PLLA thin films with a thickness of 100 (a-top, a-bottom), 200 (b-top, b-bottom), and 400 nm (c-top, c-bottom) on functionalized $SiO_2$ of SUB-3 substrates with thermal annealing for 5 min at 180 °C.**

250 nm, on whose surface is well-ordered perpendicular cylindrical domains, as revealed by the top-view phase images (Figure S2(b)). The bottom-view phase images that were obtained following oxygen plasma etching from the bottom to the top for 60 and 90 s yielded similar results (Figure S2(c) and S2(d)). These results suggest that the perpendicularly oriented cylinders span the entire film with a thickness of 400 nm. We speculate that the formed perpendicular cylinders depend strongly upon the air surface and are formed throughout the thickness of the film on the neutral substrate, whereas the thin-film morphology near the substrate is controlled by the functionalized surface. However, the effect of the neutral air surface controlled by high-temperature annealing is insignificant when the thickness of the BCP film is 600 nm (results not shown). Notably, perpendicular PLLA cylinders cannot be formed by spin-coating a thin film with a thickness of over 500 nm because the thickness in which orientation can be driven by solvent evaporation is limited. These results indicate that the initial morphology of kinetic origin is essential to the morphological evolution to stable equilibrium morphology upon thermal annealing.

**Improvement of Lateral Packing.** As demonstrated above, combining thermal treatment at 180 °C to create a neutral air surface with the use of a neutral substrate enables perpendicular PLLA cylinders of a length of up to 400 nm to be formed throughout the thickness of the film, but the degree of lateral order is low. We speculate that the low degree of lateral order following thermal annealing can be attributed to the fact that the mobility of the polymer chain does not suffice to achieve the lowest Gibbs free energy state (the stable equilibrium condition). To improve the lateral packing of the formed perpendicular PLLA cylinders in the PS-PLLA thin film, the annealing temperature was further increased up to 220 °C. As shown in Figure 10, perpendicular PLLA cylinders can still be formed in the PS-PLLA thin films at the higher temperatures. Most interestingly, the lateral order of the perpendicular PLLA cylinders can be significantly increased by increasing the annealing temperature, as shown in the insets in Figure 10, which show the fast Fourier transforms (FFT) of the SPM images that were obtained after annealing at 190, 200, 210, and 220 °C. Following annealing at 190 °C (Figure 10a) and 200 °C (Figure 10b), the FFT patterns exhibit full circles because of the low lateral order of the perpendicular PLLA cylindrical domains on the surface of the film. As the annealing temperature is increased to 210 °C (Figure 10c), the PLLA cylinders tend to pack hexagonally on the surface of the film with an improvement in

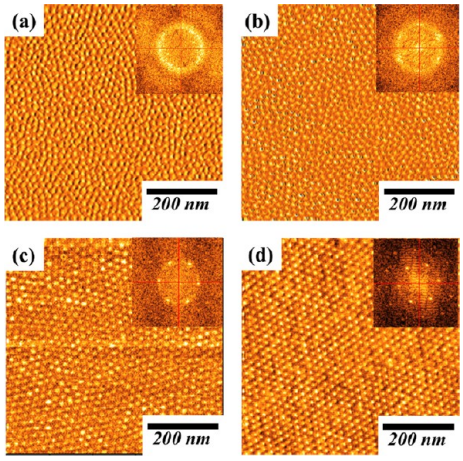


**Figure 10. Tapping-mode top-view SPM phase images of PS-PLLA thin films with a thickness of 400 nm on functionalized $SiO_2$ of SUB-3 with thermal annealing for 5 min at (a) 190, (b) 200, (c) 210, and (d) 220 °C.**

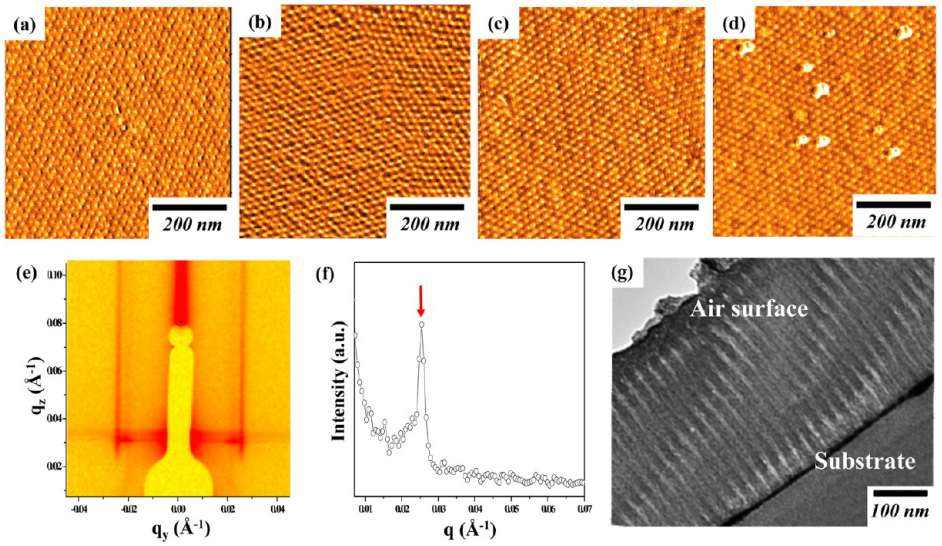


**Figure 11. Structure characterization of PS-PLLA thin film with a thickness of 400 nm on functionalized $SiO_2$ of SUB-3 after thermal annealing at 220 °C: Tapping-mode top-view SPM phase with oxygen plasma etching from top (a, b) and bottom (c, d) direction for 60 (a, c) and 90 (b, d) s. (e) 2D GISAXS pattern and (f) $q_y$ scans from 2D GISAXS pattern ($q_y$ scans were extracted at $q_z$ = 0.035 Å$^{-1}$). (g) Cross-sectional TEM image corresponding to the film in (a) to (d).**

the lateral order, so the FFT pattern exhibits reflections with approximately 6-fold symmetry.

Further increasing the annealing temperature to 220 °C (Figure 10d) yielded well-ordered PLLA cylinders that were oriented normal to the surface. The FFT pattern exhibits 6-fold symmetry with multiple higher-order reflections, suggesting the formation of hexagonally packing cylinders with long-range order. Similar results (Figure 11) were obtained using oxygen plasma etching from the top and from the bottom, as described previously, suggesting that the well-ordered perpendicular cylinders span the entire thickness of the film. The long-range perpendicular PLLA cylinders in a PS-PLLA thin film can be further identified using grazing incidence SAXS (GISAXS), which yields diffraction spots along the $q_y$ direction (Figure 11e). Figure 11f shows $q_y$ scans that were obtained from the 2D pattern. These $q_y$ scans were extracted at $q_z$ = 0.035 Å$^{-1}$. The center-to-center distance of the PLLA cylinders, approximately 26−29 nm, determined from the first-order peak is similar to that determined from the SPM image. Whereas GISAXS provides an average orientation of the microdomains in the film, transmission electron microscopy (TEM) was further used to truly demonstrate the suggested film-spanning perpendicular PLLA cylinders. Figure 11g shows a cross-sectional TEM image of PS-PLLA film after thermal treatment. The PS microdomains, selectively stained with $RuO_4$, appear dark, whereas the PLLA microdomains appear bright. As can be seen, the TEM image shows that the perpendicular cylinders extend from the film surface to the substrate and propagate through the entire 400 nm thick film. As a result, with the neutral substrate, film-spanning perpendicular PLLA cylinders in a film can be fabricated by high-temperature thermal treatment.

## CONCLUSIONS

A neutral substrate is created by two-step surface functionalization with PS-OH followed by PLLA-OH. Its surface properties can be fine-tuned by controlling the ratio of grafted PS-OH to PLLA-OH. Consequently, combining thermal treatment at high temperature to create a neutral air surface with the use of the neutral substrate enables film-spanning perpendicular PLLA cylinders in a film with sub-micrometer lengths and lateral order to be achieved by annealing of the sample at high temperature. This approach provides a simple and convenient way to control the orientation of cylindrical microdomains in BCP films. Furthermore, the formation of such cylinders in films with a well-ordered texture and sub-micrometer thickness has possible applications in gas storage, separation materials, controlled release of drugs, photovoltaics, and electrode materials for energy storage and may offer additional benefits to functional block copolymer systems.

## EXPERIMENTAL SECTION

**Materials.** Hydroxyl-terminated polystyrene (PS-OH) with $M_n$ = 10 800 g mol$^{-1}$ and polydispersity index (PDI) = 1.25 was synthesized by atom transfer radical polymerization.[62] Hydroxyl-terminated poly(L-lactide) (PLLA-OH) with $M_n$ = 10 500 g mol$^{-1}$ and PDI = 1.16 was synthesized by ring-opening polymerization.[63] The PS-PLLA was prepared by a sequential living polymerization using a double-headed initiator. The synthetic routes of the PS-PLLA sample were described in our previous publication.[63,64] The number-average molecular weight and the PDI of the PS

were determined by gel permeation chromatography (GPC). The PDI of the PS-PLLA was determined by GPC, and the number of L-LA repeating units was determined as a function of the number of styrene repeating units by $^1$H NMR analysis. The number-average molecular weights of the PS block and the PLLA block were 17300 and 9500 g mol$^{-1}$, respectively, and the PDI of the PS-PLLA was 1.33. The volume fraction of PLLA was thus calculated to be $f_{PLLA}^{v} = 0.31$ by assuming that the densities of the PS and the PLLA were 1.02 and 1.248 g cm$^{-3}$, respectively. Silicon substrate was cleaned using a piranha solution (30:70 v/v % of $H_2O_2/H_2SO_4$) at 140 °C for 30 min, followed by rinsing with deionized water and then drying in flowing $N_2$.

**Preparation of Functionalized $SiO_2$ with Mixed Homopolymer Brushes.** The 0.1 mL polymer solution (1 wt % PS-OH) in 1,2-dichloroethane was spin-coated (acceleration is 3000 rpm/s) onto a Si wafer with $SiO_2$ at 1000 rpm for 1 min. Subsequently, the Si wafer with $SiO_2$ surface that was coated with a thin layer of PS-OH was annealed at 140 °C in a vacuum oven for different periods to graft PS-OH onto the wafer. Rinsing with 1,2-dichloroethane then removed ungrafted PS-OH. The PLLA-OH was spin-coated on the functionalized $SiO_2$ with PS-OH brushes, and the film was thermally annealed at 180 °C in a vacuum oven. Finally, functionalized $SiO_2$ with mixed homopolymer brushes was obtained after rinsing with 1,2-dichloroethane to remove ungrafted PLLA-OH.

**Measurement of Contact Angle and Calculation of Surface Energy.** The work of adhesion of a thin layer of homopolymer with functionalized $SiO_2$ is generally given by[65]

$$W_{12} = 4\left(\frac{\gamma_1^d\gamma_2^d}{\gamma_1^d+\gamma_2^d}+\frac{\gamma_1^p\gamma_2^p}{\gamma_1^p+\gamma_2^p}\right)$$

where $\gamma^p$ and $\gamma^d$ are the polar and dispersion components of surface tension, respectively. In general, the surface tension of the functionalized $SiO_2$ substrate can be calculated from the measured contact angles using the geometric-mean method using the equation $(1+\cos\theta_t)\gamma_t = 2\{(\gamma_t^d\gamma_s^d)^{1/2} + (\gamma_t^p\gamma_s^p)^{1/2}\}$, where $\theta_t$ represents the contact angle of a test liquid on the functionalized $SiO_2$ substrate and $\gamma_t$ and $\gamma_s$ represent the surface tensions of the test liquid and the solid surfaces, respectively.[66] A 0.002 mL amount of water and ethylene glycol were used as testing liquids for the calculation of the polar ($\gamma_{Sub}^p$) and dispersion ($\gamma_{Sub}^d$) components of surface tension for the functionalized $SiO_2$ substrate. The resulting work of adhesion of PS with the functionalized $SiO_2$ surface; ($W_{PS\text{-}Sub}$) and the adhesion of PLLA with the functionalized $SiO_2$ surface ($W_{PLLA\text{-}Sub}$) can be calculated.

**Preparation of Samples.** Thin-film samples with different thickness were prepared on a functionalized $SiO_2$ by spin-coating (acceleration is 3000 rpm/s) at 1000 rpm for 1 min using 0.5, 1.3, 2.5, and 5 wt % chlorobenzene solution of PS-PLLA at 50 °C and then thermally annealing the films at 180, 190, 200, 210, and 220 °C in a vacuum (1 Torr) for 5 min. Notably, the neutral air surface of the PS-PLLA thin-film sample can be achieved by thermal annealing at a temperature of over 180 °C. Nevertheless, severe degradation may occur when the temperature exceeds 220 °C. The oxygen plasma treatment for oxidation was carried out by a RF power of 50 W for 60 and 90 s at the pressure of 50 mtorr. The thicknesses of thin-film samples were determined by the alpha-step, during which the thin-film sample was scratched by using a sharp knife to create a cutting edge for thickness measurement.

**Scanning Probe Microscope.** Tapping-made SPM images of thin-film samples were obtained. To examine the bottom-view morphology, thin-film samples were stripped from the functionalized $SiO_2$ substrate using 1% HF solution for 30 s and floated on the surface of water. They were then recovered using copper grids. A Seiko SPA-400 AFM with a Seiko SPI-3800N probe station was utilized at room temperature. A rectangular silicon tip was used in dynamic force mode experiments with a spring force of 5 N m$^{-1}$ and a scan rate of 1 Hz.

**X-ray Photoelectron Spectroscopy.** XPS measurements were made using a Thermo VG-Scientific Sigma Probe spectrometer that was equipped with a hemispherical electron analyzer. The operating conditions for XPS were as follows: Mg Kα anode, 15 kV, 7.2 mA; incident angle, 45°; angle of collection, 45°; analysis diameter, 400 μm.

**Transmission Electron Microscopy.** To examine the cross-sectional morphology, thin-film samples were stripped from the functionalized $SiO_2$ substrate using 1% HF solution for 30 s and floated on the surface of water. They were then picked up with a piece of polyimide thin plate. Samples were stained with $RuO_4$ by exposing the samples to the vapor of 4% aqueous $RuO_4$ solution for 3 h to increase the mass−thickness contrast before embedding with epoxy resin. The epoxy-embedded thin-film samples were microtomed normal to the film plane at a thickness of 50 nm and transferred onto a Cu grid. A JEOL JEM-2100 transmission electron microscope was used at an accelerating voltage of 200 kV.

**Grazing Incidence Small-Angle X-ray Scattering.** GISAXS was conducted at beamline BL23A1 in the National Synchrotron Radiation Research Center (NSRRC), Taiwan. A monochromatic beam with $\lambda$ = 1.033 Å was used, and the incident angle was 0.2°. Scattering intensity profiles were determined for the scattering intensity ($I$) *versus* the scattering vector ($q$), where $q = (4\pi/\lambda)\sin(\theta/2)$ and $\theta$ is the scattering angle.

*Conflict of Interest:* The authors declare no competing financial interest.

*Acknowledgment.* The financial support of the National Science Council (Grant NSC 99-2120-M-007-003 of Taiwan) is acknowledged.

*Supporting Information Available:* SPM and TEM images for PS-PLLA thin films. This information is available free of charge *via* the Internet at http://pubs.acs.org.

## REFERENCES AND NOTES

1. Bates, F. S.; Fredrickson, G. H. Block Copolymer Thermodynamics: Theory and Experiment. *Annu. Rev. Phys. Chem.* **1990**, *41*, 525–557.
2. Park, C.; Yoon, J.; Thomas, E. L. Enabling Nanotechnology with Self Assembled Block Copolymer Patterns. *Polymer* **2003**, *44*, 6725–6760.
3. Kim, G.; Libera, M. Morphological Development in Solvent-Cast Polystyrene-Polybutadiene-Polystyrene (SBS) Triblock Copolymer Thin Films. *Macromolecules* **1998**, *31*, 2569–2577.
4. Fukunaga, K.; Elbs, H.; Magerle, R.; Krausch, G. Large-Scale Alignment of ABC Block Copolymer Microdomains *via* Solvent Vapor Treatment. *Macromolecules* **2000**, *33*, 947–953.
5. Temple, K.; Kulbaba, K.; Power-Billard, K. N.; Manners, I.; Leach, A.; Xu, T.; Russell, T. P.; Hawker, C. J. Spontaneous Vertical Ordering and Pyrolytic Formation of Nanoscopic Ceramic Patterns from Poly(styrene-*b*-ferrocenylsilane). *Adv. Mater.* **2003**, *15*, 297–300.
6. Albert, J. N. L.; Young, W. S.; Lewis, R. L.; Bogart, T. D.; Smith, J. R.; Epps, T. H. Systematic Study on the Effect of Solvent Removal Rate on the Morphology of Solvent Vapor Annealed ABA Triblock Copolymer Thin Films. *ACS Nano* **2012**, *6*, 459–466.
7. Park, S.; Wang, J. Y.; Kim, B.; Chen, W.; Russell, T. P. Solvent-Induced Transition from Micelles in Solution to Cylindrical Microdomains in Diblock Copolymer Thin Films. *Macromolecules* **2007**, *40*, 9059–9063.
8. Park, S.; Kim, B.; Xu, J.; Hofmann, T.; Ocko, B. M.; Russell, T. P. Lateral Ordering of Cylindrical Microdomains under Solvent Vapor. *Macromolecules* **2009**, *42*, 1278–1284.
9. Lee, D. H.; Park, S.; Gu, W. Y.; Russell, T. P. Highly Ordered Nanoporous Template from Triblock Copolymer. *ACS Nano* **2011**, *5*, 1207–1214.
10. Keller, A.; Pedemonte, E.; Willmouth, F. M. Macro Lattice from Segregated Amorphous Phases of a Three Block Copolymer. *Nature* **1970**, *225*, 385–389.
11. Albalak, R. J.; Thomas, E. L. Microphase Separation of Block Copolymer Solutions in a Flow Field. *J. Polym. Sci., Part B: Polym. Phys.* **1993**, *31*, 37–46.
12. Koppi, K. A.; Tirrell, M.; Bates, F. S. Shear Induced Isotropic-to-Lamellar Transition. *Phys. Rev. Lett.* **1993**, *70*, 1449–1452.

13. Chen, Z. R.; Kornfield, J. A.; Smith, S. D.; Grothaus, J. T.; Satkowski, M. M. Pathways to Macroscale Order in Nanostructured Block Copolymers. *Science* **1997**, *277*, 1248–1253.
14. Albalak, R. J.; Capel, M. S.; Thomas, E. L. Solvent Swelling of Roll-Cast Triblock Copolymer Films. *Polymer* **1997**, *39*, 1647–1656.
15. Angelescu, D. E.; Waller, J. H.; Register, R. A.; Chaikin, P. M. Shear-Induced Alignment in Thin Films of Spherical Nanodomains. *Adv. Mater.* **2005**, *17*, 1878–1881.
16. Hong, Y. R.; Adamson, D. H.; Chaikin, P. M.; Register, R. A. Shear-Induced Sphere-to-Cylinder Transition in Diblock Copolymer Thin Films. *Soft Matter* **2009**, *5*, 1687–1691.
17. Morkved, T. L.; Lu, M.; Urbas, A. M.; Ehrichs, E. E.; Jaeger, H. M.; Mansky, P.; Russell, T. P. Local Control of Microdomain Orientation in Diblock Copolymer Thin Films with Electric Fields. *Science* **1996**, *273*, 931–933.
18. Thurn-Albrecht, T.; Schotter, J.; Kästle, G. A.; Emley, N.; Shibauchi, T.; Krusin-Elbaum, L.; Guarini, K.; Black, C. T.; Tuominen, M. T.; Russell, T. P. Ultrahigh-Density Nanowire Arrays Grown in Self-Assembled Diblock Copolymer Templates. *Science* **2000**, *290*, 2126–2129.
19. Olszowka, V.; Hund, M.; Kuntermann, V.; Scherdel, S.; Tsarkova, L.; Boker, A. Electric Field Alignment of a Block Copolymer Nanopattern: Direct Observation of the Microscopic Mechanism. *ACS Nano* **2009**, *3*, 1091–1096.
20. Hashimoto, T.; Bodycomb, J.; Funaki, Y.; Kimishima, K. The Effect of Temperature Gradient on the Microdomain Orientation of Diblock Copolymers Undergoing an Order-Disorder Transition. *Macromolecules* **1999**, *32*, 952–954.
21. Mita, K.; Takenaka, M.; Hasegawa, H.; Hashimoto, T. Cylindrical Domains of Block Copolymers Developed *via* Ordering under Moving Temperature Gradient: Real-Space Analysis. *Macromolecules* **2008**, *41*, 8789–8799.
22. De Rosa, C.; Park, C.; Thomas, E. L.; Lotz, B. Microdomain Patterns from Directional Eutectic Solidification and Epitaxy. *Nature* **2000**, *405*, 433–437.
23. Ho, R. M.; Hsieh, P. Y.; Tseng, W. H.; Lin, C. C.; Huang, B. H.; Lotz, B. Crystallization-Induced Orientation for Microstructures of Poly(L-lactide)-*b*-poly($\varepsilon$-caprolactone) Diblock Copolymers. *Macromolecules* **2003**, *36*, 9085–9092.
24. Park, Y. J.; Kang, S. J.; Lotz, B.; Brinkmann, M.; Thierry, A.; Kim, K. J.; Park, C. Ordered Ferroelectric PVDF-TrFE Thin Films by High Throughput Epitaxy for Nonvolatile Polymer Memory. *Macromolecules* **2008**, *41*, 8648–8654.
25. Heier, J.; Genzer, J.; Kramer, E. J.; Bates, F. S.; Walheim, S.; Krausch, G. Transfer of a Chemical Substrate Pattern into an Island-Forming Diblock Copolymer Film. *J. Chem. Phys.* **1999**, *111*, 11101–11110.
26. Rockford, L.; Liu, Y.; Mansky, P.; Russell, T. P.; Yoon, M.; Mochrie, S. G. J. Polymers on Nanoperiodic, Heterogeneous Surfaces. *Phys. Rev. Lett.* **1999**, *82*, 2602–2605.
27. Kim, S. O.; Solak, H. H.; Stoykovich, M. P.; Ferrier, N. J.; de Pablo, J. J.; Nealey, P. F. Epitaxial Self-Assembly of Block Copolymers on Lithographically Defined Nanopatterned Substrates. *Nature* **2003**, *424*, 411–414.
28. Edwards, E. W.; Montague, M. F.; Solak, H. H.; Hawker, C. J.; Nealey, P. F. Precise Control Over Molecular Dimensions of Block-Copolymer Domains Using the Interfacial Energy of Chemically Nanopatterned Substrates. *Adv. Mater.* **2004**, *16*, 1315–1319.
29. Stoykovich, M. P.; Muller, M.; Kim, S. O.; Solak, H. H.; Edwards, E. W.; de Pablo, J. J.; Nealey, P. F. Directed Assembly of Block Copolymer Blends into Nonregular Device-Oriented Structures. *Science* **2005**, *308*, 1442–1446.
30. Ruiz, R.; Kang, H. M.; Detcheverry, F. A.; Dobisz, E.; Kercher, D. S.; Albrecht, T. R.; de Pablo, J. J.; Nealey, P. F. Density Multiplication and Improved Lithography by Directed Block Copolymer Assembly. *Science* **2008**, *321*, 936–939.
31. Ji, S. X.; Nagpal, U.; Liu, G. L.; Delcambre, S. P.; Muller, M.; de Pablo, J. J.; Nealey, P. F. Directed Assembly of Non-equilibrium ABA Triblock Copolymer Morphologies on Nanopatterned Substrates. *ACS Nano* **2012**, *6*, 5440–5448.
32. Segalman, R. A.; Yokoyama, H.; Kramer, E. J. Graphoepitaxy of Spherical Domain Block Copolymer Films. *Adv. Mater.* **2001**, *13*, 1152–1155.
33. Cheng, J. Y.; Ross, C. A.; Thomas, E. L.; Smith, H. I.; Vancso, G. J. Fabrication of Nanostructures with Long-Range Order Using Block Copolymer Lithography. *Appl. Phys. Lett.* **2002**, *81*, 3657–3659.
34. Segalman, R. A.; Hexemer, A.; Kramer, E. J. Effects of Lateral Confinement on Order in Spherical Domain Block Copolymer Thin Films. *Macromolecules* **2003**, *36*, 6831–6839.
35. Cheng, J. Y.; Ross, C. A.; Thomas, E. L.; Smith, H. I.; Vancso, G. J. Templated Self-Assembly of Block Copolymers: Effect of Substrate Topography. *Adv. Mater.* **2003**, *15*, 1599–1602.
36. Cheng, J. Y.; Mayes, A. M.; Ross, C. A. Nanostructure Engineering by Templated Self-Assembly of Block Copolymers. *Nat. Mater.* **2004**, *3*, 823–828.
37. Cheng, J. Y.; Zhang, F.; Chuang, V. P.; Mayes, A. M.; Ross, C. A. Self-Assembled One-Dimensional Nanostructure Arrays. *Nano Lett.* **2006**, *6*, 2099–2103.
38. Chai, J.; Wang, D.; Fan, X. N.; Buriak, J. M. Assembly of Aligned Linear Metallic Patterns on Silicon. *Nat. Nanotechnol.* **2007**, *2*, 500–506.
39. Chai, J.; Buriak, J. M. Using Cylindrical Domains of Block Copolymers to Self-Assemble and Align Metallic Nanowires. *ACS Nano* **2008**, *2*, 489–501.
40. Bita, I.; Yang, J. K. W.; Jung, Y. S.; Ross, C. A.; Thomas, E. L.; Berggren, K. K. Graphoepitaxy of Self-Assembled Block Copolymers on Two-Dimensional Periodic Patterned Templates. *Science* **2008**, *321*, 939–943.
41. Park, S.; Lee, D. H.; Xu, J.; Kim, B.; Hong, S. W.; Jeong, U.; Xu, T.; Russell, T. P. Macroscopic 10-Terabit-per-Square-Inch Arrays from Block Copolymers with Lateral Order. *Science* **2009**, *323*, 1030–1033.
42. Tavakkoli, K. G. A.; Gotrik, K. W.; Hannon, A. F.; Alexander-Katz, A.; Ross, C. A.; Berggren, K. K. Templating Three-Dimensional Self-Assembled Structures in Bilayer Block Copolymer Films. *Science* **2012**, *336*, 1294–1298.
43. Wu, N. L. Y.; Zhang, X. J.; Murphy, J. N.; Chai, J. A.; Harris, K. D.; Buriak, J. M. Density Doubling of Block Copolymer Templated Features. *Nano Lett.* **2012**, *12*, 264–268.
44. Peters, R. D.; Yang, X. M.; Kim, T. K.; Nealey, P. F. Wetting Behavior of Block Copolymers on Self Assembled Films of Alkylchlorosiloxanes: Effect of Grafting Density. *Langmuir* **2000**, *16*, 9620–9626.
45. Peters, R. D.; Yang, X. M.; Kim, T. K.; Sohn, B. H.; Nealey, P. F. Using Self-Assembled Monolayers Exposed to X-rays to Control the Wetting Behavior of Thin Films of Diblock Copolymers. *Langmuir* **2000**, *16*, 4625–4631.
46. Han, E.; In, I.; Park, S. M.; La, Y. H.; Wang, Y.; Nealey, P. F.; Gopalan, P. Photopatternable Imaging Layers for Controlling Block Copolymer Microdomain Orientation. *Adv. Mater.* **2007**, *19*, 4448–4452.
47. Han, E.; Stuen, K. O.; Leolukman, M.; Liu, C. C.; Nealey, P. F.; Gopalan, P. Perpendicular Orientation of Domains in Cylinder-Forming Block Copolymer Thick Films by Controlled Interfacial Interactions. *Macromolecules* **2009**, *42*, 4896–4901.
48. Suh, H. S.; Kang, H.; Liu, C. C.; Nealey, P. F.; Char, K. Orientation of Block Copolymer Resists on Interlayer Dielectrics with Tunable Surface Energy. *Macromolecules* **2010**, *43*, 461–466.
49. Mansky, P.; Liu, Y.; Huang, E.; Russell, T. P.; Hawker, C. J. Controlling Polymer-Surface Interactions with Random Copolymer Brushes. *Science* **1997**, *275*, 1458–1460.
50. Huang, E.; Rockford, L.; Russell, T. P.; Hawker, C. J. Nanodomain Control in Copolymer Thin Films. *Nature* **1998**, *395*, 757–758.
51. Huang, E.; Russell, T. P.; Harrison, C.; Chaikin, P. M.; Register, R. A.; Hawker, C. J.; Mays, J. Using Surface Active Random Copolymers to Control the Domain Orientation in Diblock Copolymer Thin Films. *Macromolecules* **1998**, *31*, 7641–7650.
52. Ryu, D. Y.; Shin, K.; Drockenmuller, E.; Hawker, C. J.; Russell, T. P. A Generalized Approach to the Modification of Solid Surfaces. *Science* **2005**, *308*, 236–239.

53. Shengxiang, J.; Guoliang, L.; Zheng, F.; Craig, G. S. W.; Himpsel, F. J.; Nealey, P. F. Preparation of Neutral Wetting Brushes for Block Copolymer Films from Homopolymer Blends. *Adv. Mater.* **2008**, *20*, 3054–3060.
54. Mansky, P.; Russell, T. P.; Hawker, C. J.; Mays, J.; Cook, D. C.; Satija, S. K. Interfacial Segregation in Disordered Block Copolymers: Effect of Tunable Surface Potentials. *Phys. Rev. Lett.* **1997**, *79*, 237–240.
55. Gu, W.; Hong, S. W.; Russell, T. P. Orienting Block Copolymer Microdomains with Block Copolymer Brushes. *ACS Nano* **2012**, *6*, 10250–10257.
56. Ho, R. M.; Tseng, W. H.; Fan, H. W.; Chiang, Y. W.; Lin, C. C.; Ko, B. T.; Huang, B. H. Solvent-Induced Microdomain Orientation in Polystyrene-*b*-poly(L-lactide) Diblock Copolymer Thin Films for Nanopatterning. *Polymer* **2005**, *46*, 9362–9377.
57. Tseng, Y. T.; Tseng, W. H.; Lin, C. H.; Ho, R. M. Fabrication of Double-Length-Scale Patterns *via* Lithography, Block Copolymer Templating, and Electrodeposition. *Adv. Mater.* **2007**, *19*, 3584–3588.
58. Ho, R. M.; Chiang, Y. W.; Chen, C. K.; Wang, H. W.; Hasegawa, H.; Akasaka, S.; Thomas, E. L.; Burger, C.; Hsiao, B. S. Block Copolymers with a Twist. *J. Am. Chem. Soc.* **2009**, *131*, 18533–18542.
59. Minko, S.; Patil, S.; Datsyuk, V.; Simon, F.; Eichhorn, K. J.; Motornov, M.; Usov, D.; Tokarev, I.; Stamm, M. Synthesis of Adaptive Polymer Brushes via "Grafting to" Approach from Melt. *Langmuir* **2002**, *18*, 289–296.
60. Zuwei, M.; Changyou, G.; Jian, J.; Jiacong, S. Protein Immobilization on the Surface of Poly-L-lactic Acid Films for Improvement of Cellular Interactions. *Eur. Polym. J.* **2002**, *38*, 2279–2284.
61. Chen, D. J.; Gong, Y. M.; Huang, H. Y.; He, T. B.; Zhang, F. J. Competition of lamellar Orientation in Thin Films of a Symmetric Poly(styrene)-*b*-Poly(L-lactide)Diblock Copolymer in Melt State. *Macromolecules* **2007**, *40*, 6631–6637.
62. Olayo-Valles, R.; Guo, S.; Lund, M. S.; Leighton, C.; Hillmyer, M. A. Perpendicular Domain Orientation in Thin Films of Polystyrene−Polylactide Diblock Copolymers. *Macromolecules* **2005**, *38*, 10101–10108.
63. Ho, R. M.; Chen, C. K.; Chiang, Y. W.; Ko, B. T.; Lin, C. C. Tubular Nanostructures from Degradable Core-Shell Cylinder Microstructures in Chiral Diblock Copolymers. *Adv. Mater.* **2006**, *18*, 2355–2358.
64. Ho, R. M.; Chiang, Y. W.; Tsai, C. C.; Lin, C. C.; Ko, B. T.; Huang, B. H. Three-Dimensionally Packed Nanohelical Phase in Chiral Block Copolymers. *J. Am. Chem. Soc.* **2004**, *126*, 2704–2705.
65. Wu, S. *Polymer Interface and Adhesion*; Marcel Dekker: New York, 1982; Chapter 5.
66. Owens, D. K.; Wendt, R. C. Estimation of Surface Energy of Polymers. *J. Appl. Polym. Sci.* **1969**, *13*, 1741–1747.